Advances in Aircraft and Spacecraft Science, *Vol. 12, No. 2 (2025) 95-115*
https://doi.org/10.12989/aas.2025.12.2.095

Micromechanical model-based analysis of porous functionally graded plates behavior using refined higher-order theory

Belkacem Adim*[1,2], Tahar Hassaine Daouadji[2,3] and Kheira Bekda[1]

[1]*Civil, Mechanical and Transportation Engineering Department, Tissemsilt University, Tissemsilt 38000, Algeria*
[2]*Geomatics and Sustainable Development Laboratory, Ibn Khaldoun University, Tiaret 14000, Algeria*
[3]*Civil Engineering Department, Ibn Khaldoun University, Tiaret14000, Algeria*

(Received January 29, 2025, Revised May 6, 2025, Accepted May 8, 2025)

Abstract. This manuscript investigates the impact of porosity and micromechanical models on the flexural behavior of functionally graded plates employing a refined higher order shear and deformation theory. The plate's material properties are supposed to be varying gradually through the direction of the plate's thickness according to different micromechanical models namely: Voigt's model often used in furthermost functionally graded plates researches, Mori Tanaka's, Reuss's and LRVE's models. Virtual works principle is employed to determine the equations of equilibrium and some numerical results are exhibited to validate the accuracy and effectiveness of the present theory for flexural behavior of functionally graded plates. A parametric investigation is conducted to assess the influence of various parameters on the displacements and stresses of the plate including micromechanical models', porosity distribution shape and geometry of the plate. In light of this study we conclude that the present refined theory is efficient accurate and reliable for predicting the flexural behavior of functionally graded plates considering different porosity distribution shapes and various micromechanical models.

Keywords: flexural behavior; functionally graded plates; micromechanical models; porosity distribution shapes; shear stresses and strains

1. Introduction

Functionally Graded Materials (FGM) provide superior mechanical properties relative to conventional homogeneous materials thanks to their distinctive compositional gradients, enabling customized performance across diverse applications. FGMs can be engineered to combine dissimilar materials, optimizing their mechanical responses under specific conditions, such as thermal or mechanical stress, which is mainly beneficial in numerous fields (Naebe and Shirvanimoghaddam 2016, Silva *et al.* 2024). Furthermore, improvements in manufacturing processes like additive manufacturing make it easier to precisely manage material gradients, which lowers concentrations of stress and improves the ability to bear loads (Daouadji and Adim 2016). All things considered, FGMs are a major breakthrough in material science, offering solutions that conventional homogenous materials are unable to provide (Naveen and Devarajaiah 2024, Zghal and Dammak 2024).

*Corresponding author, Associate Professor, E-mail: adim.belkacem@univ-tissemsilt.dz

http://www.techno-press.org/?journal=aas&subpage=7 ISSN: 2287-528X (Print), 2287-5271 (Online)

Functionally graded materials in structural applications have recently advanced, with an emphasis on improving their mechanical and thermal characteristics through creative design and analysis methods (Chen *et al.* 2021, Li *et al.* 2024). According to research, FGMs, with a constant variation in material composition, are capable of overcoming challenges like delamination and cracking that are frequently observed in conventional composite structures (Li *et al.* 2019). The mechanical, thermomechanical and thermoelastic behavior of these plates under various loading conditions has been predicted using sophisticated modeling techniques, such as finite element analysis and different homogenization techniques (Abouelregal and Datrgail 2023, Li *et al.* 2025, Abouelregal and Mohamed 2018, Abouelregal, 2022).

Bending behavior of Functionally Graded Materials under mechanical loads has been thoroughly investigated using a multitude of approaches, such as experimental and finite element analysis. Significant differences in performance based on gradient profiles were found when Noori *et al.* (2024) investigated the impact of material gradient indices on the deflection and stress responses of FGM rectangular plates under various loading conditions. In their study on functionally graded viscoelastic materials, Njim *et al.* (2023) showed that while changes in power-law exponents can improve fatigue strength, greater porosity has a detrimental effect on bending strength and deflection. With a focus on the impact of material distribution on structural reactions under mechanical loads, Bui *et al.* (2022) examined the geometrically nonlinear response of FG beams.

Numerous investigations have shown that the behavior of Functionally Graded Materials is greatly influenced by variations in material properties through their thickness. A gradual change in material properties enables FGMs to combine the advantages of several materials, impacting deformation and stress responses subjected to different loading and boundary conditions. For example, Noori *et al.* showed that, depending on boundary and loading conditions, varying material gradients in FGM plates result in differences in deflection and stress (Noori *et al.* 2024). According to the study of Adıyaman and Turan (2024) of porous 2D FG beams, porosity and how it is distributed have a significant impact on static analysis, affecting stresses and deformations. In their investigation of multidirectional FG plates with varying thickness, Son and Qui (2022) demonstrated how material gradation, as determined by Isogeometric analysis, influences vibration and static bending behavior. A power-law method was used to determine the effective properties. According to Sahmani *et al.* (2021) flexural stiffness in FG nanoplates is influenced by the thickness variation shape (concave, convex or linear) because of surface elasticity; variations in the thickness pattern vary the stiffness and deflection outcomes. Ghazzawi and Abdelrahman (2020) compared various property distribution functions, including sigmoid and exponential variations, demonstrating that these variations impact the shear deformation effects and bending behavior in thick FGM plates, with sigmoid FGMs exhibiting less noticeable stiffening than power-law FGMs.

Recent developments in micromechanical models for functionally graded materials (FGM) have aimed at improving the accuracy of predictions regarding mechanical and thermomechanical behaviors across diverse conditions. Several micromechanical models, such as Voigt, Reuss, Tamura, LRVE, and Hashin, have been employed to predict the material properties of FGMs, particularly in the context of simply-supported plates. These models are crucial for understanding the free vibration and static behavior of FGMs, especially when analyzed using quasi-3D hyperbolic shear deformation theory, which considers stretching effects and temperature influences on fundamental frequencies and transverse displacements (Chen *et al.* 2024). Moreover, the Green's function technique has been employed to compute local fields in functionally graded

materials under thermomechanical loading, facilitating the prediction of effective material properties. This approach, combined with Eshelby's equivalent inclusion method, provides a detailed analysis of the effects of particle size and material gradation on the effective stiffness, thermal expansion coefficient, and heat conductivity of FGM (Wu *et al.* 2024). Furthermore, advanced thermoelastic models incorporating higher-order fractional derivatives have been developed to analyze the thermoelastic behavior of FGMs, particularly under thermal shock conditions. These models use the dual-phase-lag thermos-elasticity theory to provide sophisticated approximations of heat flux, temperature gradients, and thermal displacements (Alsaeed and Abouelregal 2024). In addition, the variation of material properties in multiple directions in functionally graded materials (FGMs) poses challenges in estimating overall mechanical properties, leading to the development of various modelling techniques to address these complexities (Joshi *et al.* 2022).

Porosity variations have a major effect on the bending behavior of FG materials, affecting deflection, stress distribution, and overall mechanical performance. It is possible to enhance structural integrity by carefully managing the changed neutral plane deformation and stress concentrations caused by porous imperfections, which can decrease bending strength while increasing compressive strength (Nadiia and Jia 2024). Stochastic models offer insights into material unpredictability, and the study of curved FG beams shows that bending behaviors under uniform loads are influenced by various porosity distributions, including even and sinusoidal (Amir *et al.* 2024). Porosity distribution and gradation parameters also affect the bending and buckling responses of porous beams; exponential changes in material characteristics have a significant impact on deflections and critical buckling loads (Adıyaman and Turan 2024). According to Sidda and Vijaya (2024), porosity plays a crucial role in determining the mechanical characteristics and buckling behavior of functionally graded porous plates. This highlights the importance of carefully considering porosity in design and analysis, as higher porosity decreases the critical buckling load, demonstrating that higher porosity weakens the material's structural integrity by causing voids that impair its capacity to support forces of compression. As stated by Masmoudi *et al.* (2024), porosity is a significant factor that needs to be addressed while designing FG sandwich plates. It is crucial for engineering applications as an understanding of its impacts can improve predictions of stability and performance under different loading scenarios.

As we learned from this bibliographic review, it is rare to find thorough studies which investigate all of the different facets of the behavior of functionally graded plates at the same time, especially when it comes to examining how the choice of micromechanical models affects the bending behavior of functionally graded plates using refined high order shear deformation theory.

For the engineering community, researching how porosity and micromechanical models affect functionally graded material (FGM) plates has several useful applications. These investigations shed light on the mechanical behavior of FGMs, which is essential for creating cutting-edge materials with specific qualities for particular uses. Engineers may improve material performance under a variety of conditions, including mechanical and temperature loadings, by understanding how porosity and micromechanical models affect FGM plates. Such knowledge is crucial for creating more dependable and efficient materials in sectors including civil, automotive, and aerospace engineering.

The primary goal of this study is to investigate how micromechanical models affect the bending behavior of porous functionally graded plates using the present refined high order shear deformation theory, this refined theory takes into account the shear effect on the deformations and stresses without needing any shear correction factor (such as, the first order shear deformation

theory), moreover the present theory includes only four unknown variables against five unknowns or more in the other high order theories, which makes this theory advantageous compared to other theories in terms of simplifying the mathematical formulation and time gaining.

2. Micromechanical models considered for imperfect FG plates

In this manuscript we study an FG plate with length "*a*", width "*b*" and thickness "*h*". The materials characteristics of the functionally graded plate vary progressively from 100% metal in the lower surface to 100% ceramic in the upper surface. The Young's modulus $E(z)$ of the FGM plate is determined by the various micromechanical models given bellow.

Where E_c and E_m denotes the material properties of ceramic and metal, respectively, and "β" is the material's volume fraction exponent.

2.1 Voigt's model

The majority of researchers use this micromechanical model to describe materials properties distribution across the plate's thickness, this is due to its simplicity, it is given as fellow (Bouazza *et al.* 2024, Kim and Reddy 2013)

$$E(z) = E_m + (E_c - E_m)\left(\frac{1}{2} + \frac{z}{h}\right)^{\beta} - E_{porosity} \tag{1}$$

2.2 Reuss's model

the stress is supposed to be uniform across the material according Reuss (Billel 2023), this allowed him to determine the effective material properties by

$$E(z) = \frac{E_c E_m}{E_c\left(1-\left(\frac{1}{2}+\frac{z}{h}\right)^{\beta}\right)+E_m\left(\frac{1}{2}+\frac{z}{h}\right)^{\beta}} - E_{porosity} \tag{2}$$

2.3 Mori-Tanaka's model

Micromechanical models like the Mori-Tanaka model can be used to estimate the local effective material characteristics. According to this approach, the heterogeneous material is a two-phase composite made up of a matrix that is dispersed randomly and reinforced by spherical particles all over the plate. The material properties are described in accordance with the Mori-Tanaka homogenization method by (Zaoui *et al.* 2022)

$$E(z) = E_m + (E_c - E_m)\left(\frac{\left(\frac{1}{2}+\frac{z}{h}\right)^{\beta}}{1+\left(1-\left(\frac{1}{2}+\frac{z}{h}\right)^{\beta}\right)\left(\frac{E_c}{E_m}-1\right)\frac{(1+\nu)}{(3-3\nu)}}\right) - E_{porosity} \tag{3}$$

2.4 LRVE's model

To determine the FGM's effective material properties, Rabai used the LRVE (local cubic

Table 1 Types of porosity adopted in the present study

Designation of porosity	Mathematical formulation*	Shape of porosity
Type I (Uniform Distribution)	$E = (E_c - E_m)((\frac{z}{h} + 0.5))^{\beta} + E_m - (E_c + E_m)\frac{\alpha}{2}$	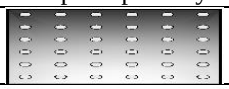
Type II (Distribution in "X" shape)	$E = (E_c - E_m)((\frac{z}{h} + 0.5))^{\beta} + E_m - (E_c + E_m)\frac{\alpha}{2}(2\frac{\lvert z\rvert}{h})$	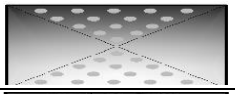
Type III (Distribution in "O" shape)	$E = (E_c - E_m)((\frac{z}{h} + 0.5))^{\beta} + E_m - (E_c + E_m)\frac{\alpha}{2}(1 - 2\frac{\lvert z\rvert}{h})$	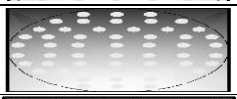
Type IV (Distribution in "V" shape)	$E = (E_c - E_m)((\frac{z}{h} + 0.5))^{\beta} + E_m - (E_c + E_m)\frac{\alpha}{2}(\frac{1}{2} + \frac{z}{h})$	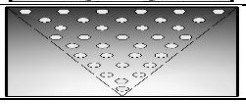

* We consider in this study that the porosity volume fraction α equal to 0.2

representative volume elements) model. The LRVE micromechanical model-based material properties can be obtained according to Billel (2023) by

$$E(z) = E_m\left(1 + \frac{\left(\frac{1}{2}+\frac{z}{h}\right)^{\beta}}{\frac{1}{1-\frac{E_m}{E_c}}\sqrt[3]{\left(\frac{1}{2}+\frac{z}{h}\right)^{\beta}}}\right) - E_{porosity} \tag{4}$$

3. Porosity distribution shape across imperfect FGM plate

In this study, the porous FGM plate is considered to have porosities spreading throughout the plate's thickness caused by flaws occurred in the manufacturing process. Typical manufacturing flaws that cause porosity in functionally graded materials (FGMs) include shrinkage during cooling, gas occlusions, and inadequate filling of reinforcing capillaries. According to Gawdzińska *et al.* (2001), inadequate filling happens when the liquid matrix does not sufficiently soak the reinforcement, frequently as a result of insufficient pressure during the casting process. This can lead to several forms of porosity. Furthermore, voids may be produced by the release of dissolved gasses during solidification, and cavities may emerge as the material changes from a liquid to a solid due to shrinkage porosity, which occurs when the cooling process is not well controlled. To be thorough, four types of porosity distributions are employed in the present investigation to cover any case scenarios that represents accurately the actual structure of porous FG plates.

In order to calculate the effective mechanical properties of imperfect FGM plate, we subtract the porosity rate ($E_{porosity}$) from the given micromechanical equation

The following table gives the main forms of porosity adopted in the present research with their graphical presentations and mathematical expressions (Daouadji *et al.* 2016a, Hadj *et al.* 2021).

4. Mathematical formulation of the present theory

In this study we examine an FG plate with dimension: "*h*" thickness, "*a*" length and "*b*" width.

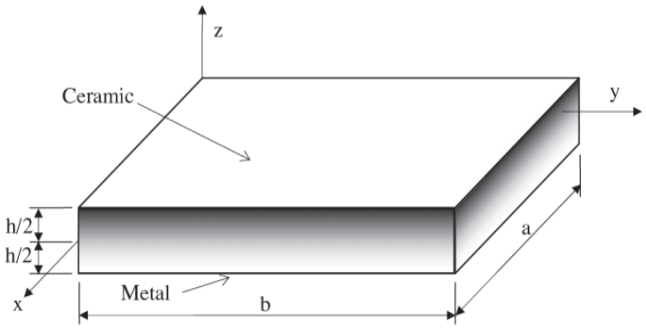

Fig. 1 Schematic of an FG plate

It is supposed that the material's characteristics will gradually change across the FG plate's thickness. The "*xy*" plane is thought to represent the plate's mid-plane, and the "z" axis is positive upward from the plate's mid-height (Fig. 1) (Adim and Daouadji 2024).

4.1 Displacements and deformations

For the development of the present theory, we assume the displacement field to be writing as follow (Henni *et al.* 2021)

$$\begin{gathered} u(x,y,z) = u_0(x,y) - z\frac{\partial w_b}{\partial x} - f(z)\frac{\partial w_s}{\partial x} \\ v(x,y,z) = v_0(x,y) - z\frac{\partial w_b}{\partial y} - f(z)\frac{\partial w_s}{\partial y} \\ w(x,y,z) = w_b(x,y) + w_s(x,y) \end{gathered} \tag{5a}$$

The shape function describing the distribution across the thickness of the plate of shear stresses and strains is represented according to Li *et al.* (2020) in Eq. (5b), while the displacements in the mid-plane section u_0 and v_0 of the plate are in the "*x*" and "*y*" directions, respectively; w_b and w_s are the bending and shear components of transverse displacement.

$$f(z) = z - (\frac{h}{\pi})sin(\frac{\pi z}{h}) \tag{5b}$$

With only four unknown variables compared to five or more in other high order theories, the present refined high order theory accounts for the shear effect on the stresses and deformations by ensuring a parabolic distribution of shear stresses across the plate's thickness while guaranteeing the nullity of these stresses at the top and bottom of the FG plate without requiring any shear correction factors. This makes the theory more effective compared to other high order theories in terms of optimizing the mathematical formulation and saving time.

The deformations relations can be attained by deriving the field of displacement shown in Eq. 5a, these stains can be given by

$$\varepsilon_x = \frac{\partial u_0}{\partial x} - z\frac{\partial^2 w_b}{\partial x^2} - f(z)\frac{\partial^2 w_s}{\partial x^2} \tag{6a}$$

$$\varepsilon_y = \frac{\partial v_0}{\partial y} - z\frac{\partial^2 w_b}{\partial y^2} - f(z)\frac{\partial^2 w_s}{\partial y^2} \tag{6b}$$

$$\varepsilon_z = 0 \tag{6c}$$

$$\gamma_{xy} = \frac{\partial u_0}{\partial y} + \frac{\partial v_0}{\partial x} - 2z\frac{\partial^2 w_b}{\partial x \partial y} - 2f(z)\frac{\partial^2 w_s}{\partial x \partial y} \tag{6d}$$

$$\gamma_{yz} = g(z)\frac{\partial w_s}{\partial y} \tag{6e}$$

$$\gamma_{xz} = g(z)\ \frac{\partial w_s}{\partial x} \tag{6f}$$

By assuming the following expressions

$$\varepsilon_x^0 = \frac{\partial u_0}{\partial x},\ k_x^b = -\frac{\partial^2 w_b}{\partial x^2},\ k_x^s = -\frac{\partial^2 w_s}{\partial x^2}, \varepsilon_y^0 = \frac{\partial v_0}{\partial y},\ k_y^b = -\frac{\partial^2 w_b}{\partial y^2}, \tag{6g}$$

$$k_y^s = -\frac{\partial^2 w_s}{\partial y^2}\ \ \gamma_{xy}^0 = \frac{\partial u_0}{\partial y} + \frac{\partial v_0}{\partial x},\ k_{xy}^b = -2\frac{\partial^2 w_b}{\partial x \partial y},\ k_{xy}^s = -2\frac{\partial^2 w_s}{\partial x \partial y}, \tag{6h}$$

$$\gamma_{yz}^s = \frac{\partial w_s}{\partial y},\ \gamma_{xz}^s = \frac{\partial w_s}{\partial x} \text{ and } g(z) = 1 - \frac{df(z)}{dz} \tag{6i}$$

The deformations can be given in the final expression by

$$\varepsilon_x = \varepsilon_x^0 + z\ k_x^b + f(z)k_x^s, \varepsilon_y = \varepsilon_y^0 + z\ k_y^b + f(z)k_y^s, \varepsilon_z = 0 \tag{6j}$$

$$\gamma_{xy} = \gamma_{xy}^0 + z\ k_{xy}^b + f(z)\ k_{xy}^s,\ \ \gamma_{yz} = g(z)\ \gamma_{yz}^s,\ \ \gamma_{xz} = g(z)\ \gamma_{xz}^s \tag{6k}$$

4.2 Stress relations

The stress relations of FG plates can be obtained using the Hooke's law, and can be written by

$$\begin{Bmatrix}\sigma_x\\ \sigma_y\\ \tau_{xy}\end{Bmatrix} = \begin{bmatrix}Q_{11} & Q_{12} & 0\\ Q_{12} & Q_{22} & 0\\ 0 & 0 & Q_{66}\end{bmatrix}\begin{Bmatrix}\varepsilon_x\\ \varepsilon_y\\ \gamma_{xy}\end{Bmatrix} \tag{7a}$$

$$\begin{Bmatrix}\tau_{yz}\\ \tau_{xz}\end{Bmatrix} = \begin{bmatrix}Q_{44} & 0\\ 0 & Q_{55}\end{bmatrix}\begin{Bmatrix}\gamma_{yz}\\ \gamma_{xz}\end{Bmatrix} \tag{7b}$$

Knowing that $(\sigma_x, \sigma_y, \tau_{xy}, \tau_{yz}, \tau_{xz})$ and $(\varepsilon_x, \varepsilon_y, \gamma_{xy}, \gamma_{yz}, \gamma_{xz})$ are the normal and shear stresses and strains components, respectively. Basing on the micromechanical material properties shown in Eq. (1) to Eq. (4), the coefficients of stiffness, Q_{ij}, can be given as

$$Q_{11} = Q_{22} = \frac{E(z)}{1-\nu^2}, Q_{12} = \frac{\nu E(z)}{1-\nu^2}, Q_{44} = Q_{55} = Q_{66} = \frac{E(z)}{2(1+\nu)} \tag{8}$$

4.3 Equations of equilibrium

The equations of equilibrium are obtained using the virtual works principle. The virtual displacements principle is given in the following formula

$$\int_V \sigma_{ij}\delta\varepsilon_{ij}dV - \int_A q\delta w dA = 0 \tag{9}$$

Where "*V*" is the plate's volume and "*A*" is its top surface. By replacing Eq. (6) and Eq. (7) into Eq. (9) and integrating this last one, Eq. (9) will result in the following expression

$$\begin{aligned}\int_A [N_x\ \delta\varepsilon_x^0 + N_y\delta\varepsilon_y^0 + N_{xy}\delta\gamma_{xy}^0 + M_x^b\delta k_x^b + M_y^b\delta k_y^b + M_{xy}^b\delta k_{xy}^b + M_x^s\delta k_x^s + M_y^s\delta k_y^s +\\ M_{xy}^s\delta k_{xy}^s + Q_{xz}^s\delta\gamma_{xz}^s + Q_{yz}^s\delta\gamma_{yz}^s]dA - \int_A q\ (\delta w_b + \delta w_s)dA = 0\end{aligned} \tag{10}$$

Where the N, M, and S^s resultants are given by

$$\begin{Bmatrix} N_x \\ N_y \\ N_{xy} \\ M_x^b \\ M_y^b \\ M_{xy}^b \\ M_x^s \\ M_y^s \\ M_{xy}^s \end{Bmatrix} = \int_{-h/2}^{h/2} \begin{Bmatrix} \sigma_x \\ \sigma_y \\ \tau_{xy} \\ z\sigma_x \\ z\sigma_y \\ z\tau_{xy} \\ f(z)\sigma_x \\ f(z)\sigma_y \\ f(z)\tau_{xy} \end{Bmatrix} dz = \begin{bmatrix} A_{11} & A_{12} & 0 & B_{11} & B_{12} & 0 & B_{11}^s & B_{12}^s & 0 \\ A_{12} & A_{22} & 0 & B_{12} & B_{22} & 0 & B_{12}^s & B_{22}^s & 0 \\ 0 & 0 & A_{66} & 0 & 0 & B_{66} & 0 & 0 & B_{66}^s \\ B_{11} & B_{12} & 0 & D_{11} & D_{12} & 0 & D_{11}^s & D_{12}^s & 0 \\ B_{12} & B_{22} & 0 & D_{12} & D_{22} & 0 & D_{12}^s & D_{22}^s & 0 \\ 0 & 0 & B_{66} & 0 & 0 & D_{66} & 0 & 0 & D_{66}^s \\ B_{11}^s & B_{12}^s & 0 & D_{11}^s & D_{12}^s & 0 & H_{11}^s & H_{12}^s & 0 \\ B_{12}^s & B_{22}^s & 0 & D_{12}^s & D_{22}^s & 0 & H_{12}^s & H_{22}^s & 0 \\ 0 & 0 & B_{66}^s & 0 & 0 & D_{66}^s & 0 & 0 & H_{66}^s \end{bmatrix} \begin{Bmatrix} \varepsilon_x^0 \\ \varepsilon_y^0 \\ \gamma_{xy}^0 \\ k_x^b \\ k_y^b \\ k_{xy}^b \\ k_x^s \\ k_y^s \\ k_{xy}^s \end{Bmatrix} \tag{11a}$$

$$\begin{Bmatrix} S_{yz}^s \\ S_{xz}^s \end{Bmatrix} = \int_{-h/2}^{h/2} g(z) \begin{Bmatrix} \tau_{yz} \\ \tau_{yz} \end{Bmatrix} dz = \begin{bmatrix} A_{44}^s & 0 \\ 0 & A_{55}^s \end{bmatrix} \begin{Bmatrix} \gamma_{yz}^s \\ \gamma_{xz}^s \end{Bmatrix} \tag{11b}$$

Knowing that A_{ij}, B_{ij}, D_{ij} etc., are the stiffness of the FG plate, expressed as

$$\begin{Bmatrix} A_{11} & B_{11} & D_{11} & B_{11}^s & D_{11}^s & H_{11}^s \\ A_{12} & B_{12} & D_{12} & B_{12}^s & D_{12}^s & H_{12}^s \\ A_{66} & B_{66} & D_{66} & B_{66}^s & D_{66}^s & H_{66}^s \end{Bmatrix} = \int_{-h/2}^{h/2} (1, z, z^2, f(z), zf(z), f^2(z)) \begin{Bmatrix} Q_{11} \\ Q_{12} \\ Q_{66} \end{Bmatrix} dz \tag{12a}$$

$$(A_{22}, B_{22}, D_{22}, B_{22}^s, D_{22}^s, H_{22}^s) = (A_{11}, B_{11}, D_{11}, B_{11}^s, D_{11}^s, H_{11}^s) \tag{12b}$$

$$A_{44}^s = A_{55}^s = \int_{-h/2}^{h/2} Q_{44} (g(z))^2 dz = \int_{-h/2}^{h/2} Q_{55} (g(z))^2 dz \tag{12c}$$

The equilibrium equations can be obtained by integrating the displacement in Eq. (9) and assuming the nullity of the coefficients δu_0, δv_0, δw_b and δw_s. Consequently, the equilibrium equations can result in

$$\delta u_0: \quad \frac{\partial N_x}{\partial x} + \frac{\partial N_{xy}}{\partial y} = 0 \tag{13a}$$

$$\delta v_0: \quad \frac{\partial N_{xy}}{\partial x} + \frac{\partial N_y}{\partial y} = 0 \tag{13b}$$

$$\delta w_b: \quad \frac{\partial^2 M_x^b}{\partial x^2} + 2\frac{\partial^2 M_{xy}^b}{\partial x \partial y} + \frac{\partial^2 M_y^b}{\partial y^2} + q = 0 \tag{13c}$$

$$\delta w_s: \quad \frac{\partial^2 M_x^s}{\partial x^2} + 2\frac{\partial^2 M_{xy}^s}{\partial x \partial y} + \frac{\partial^2 M_y^s}{\partial y^2} + \frac{\partial S_{xz}^s}{\partial x} + \frac{\partial S_{yz}^s}{\partial y} + q = 0 \tag{13d}$$

Substituting from Eq. (11a) and Eq. (11b) into Eqs. (13a)-(13d), we get

$$A_{11}\frac{\partial^2 u_0}{\partial x^2} + A_{66}\frac{\partial^2 u_0}{\partial y^2} + (A_{12} + A_{66})\frac{\partial^2 v_0}{\partial x \partial y} - B_{11}\frac{\partial^3 w_b}{\partial x^3} - (B_{12} + 2B_{66})\frac{\partial^3 w_b}{\partial x \partial y^2} - (B_{12}^s + 2B_{66}^s)\frac{\partial^3 w_s}{\partial x \partial y^2} - B_{11}^s\frac{\partial^3 w_s}{\partial x^3} = 0 \tag{14a}$$

$$A_{22}\frac{\partial^2 v_0}{\partial y^2} + A_{66}\frac{\partial^2 v_0}{\partial x^2} + (A_{12} + A_{66})\frac{\partial^2 u_0}{\partial x \partial y} - B_{22}\frac{\partial^3 w_b}{\partial y^3} - (B_{12} + 2B_{66})\frac{\partial^3 w_b}{\partial x^2 \partial y} - (B_{12}^s + 2B_{66}^s)\frac{\partial^3 w_s}{\partial x^2 \partial y} - B_{22}^s\frac{\partial^3 w_s}{\partial y^3} = 0 \tag{14b}$$

$$B_{11}\frac{\partial^3 u_0}{\partial x^3}+(B_{12}+2B_{66})\frac{\partial^3 u_0}{\partial x\partial y^2}+(B_{12}+2B_{66})\frac{\partial^3 v_0}{\partial x^2\partial y}+B_{22}\frac{\partial^3 v_0}{\partial y^3}-D_{11}\frac{\partial^4 w_b}{\partial x^4}-2(D_{12}+2D_{66})\frac{\partial^4 w_b}{\partial x^2\partial y^2}-D_{22}\frac{\partial^4 w_b}{\partial y^4}-D_{11}^s\frac{\partial^4 w_s}{\partial x^4}-2(D_{12}^s+2D_{66}^s)\frac{\partial^4 w_s}{\partial x^2\partial y^2}-D_{22}^s\frac{\partial^4 w_s}{\partial y^4}+q=0 \tag{14c}$$

$$B_{11}^s\frac{\partial^3 u_0}{\partial x^3}+(B_{12}^s+2B_{66}^s)\frac{\partial^3 u_0}{\partial x\partial y^2}+(B_{12}^s+2B_{66}^s)\frac{\partial^3 v_0}{\partial x^2\partial y}+B_{22}^s\frac{\partial^3 v_0}{\partial y^3}-D_{11}^s\frac{\partial^4 w_b}{\partial x^4}-2(D_{12}^s+2D_{66}^s)\frac{\partial^4 w_b}{\partial x^2\partial y^2}-D_{22}^s\frac{\partial^4 w_b}{\partial y^4}-H_{11}^s\frac{\partial^4 w_s}{\partial x^4}-2(H_{12}^s+2H_{66}^s)\frac{\partial^4 w_s}{\partial x^2\partial y^2}-H_{22}^s\frac{\partial^4 w_s}{\partial y^4}+A_{55}^s\frac{\partial^2 w_s}{\partial x^2}+A_{44}^s\frac{\partial^2 w_s}{\partial y^2}+q=0 \tag{14d}$$

4.4 Navier's analytical solution for FG plates

For the present research, we consider a simply supported FG plate subjected to a transverse load q. Basing on Navier's solution, we assume the following expansions of displacements (u_0; v_0, w_b; w_s) as (Adim *et al.* 2016)

$$u_0(x,y)=\sum_{m=1}^{\infty}\sum_{n=1}^{\infty}U_{mn}\,cos(\lambda x)\,sin(\mu y) \tag{15a}$$

$$v_0(x,y)=\sum_{m=1}^{\infty}\sum_{n=1}^{\infty}V_{mn}\,sin(\lambda x)\,cos(\mu y) \tag{15b}$$

$$w_b(x,y)=\sum_{m=1}^{\infty}\sum_{n=1}^{\infty}W_{bmn}\,sin(\lambda x)\,sin(\mu y) \tag{15c}$$

$$w_s(x,y)=\sum_{m=1}^{\infty}\sum_{n=1}^{\infty}W_{smn}\,sin(\lambda x)\,sin(\mu y) \tag{15d}$$

Where U_{mn}, V_{mn}, W_{bmn} and W_{smn} are unknown variables to be determined, and $\lambda=\frac{m\pi}{a}$ and $\mu=\frac{n\pi}{b}$.

The applied transverse load q is given as follows

$$q(x,y)=\sum_{m=1}^{\infty}\sum_{n=1}^{\infty}Q_{mn}\,sin(\lambda x)\,sin(\mu y) \tag{16}$$

Substituting from Eq. (15) into Eq. (14), we obtain the subsequent operator equations

$$\begin{bmatrix}a_{11}&a_{12}&a_{13}&a_{14}\\a_{12}&a_{22}&a_{23}&a_{24}\\a_{13}&a_{23}&a_{33}&a_{34}\\a_{14}&a_{24}&a_{34}&a_{44}\end{bmatrix}\begin{Bmatrix}U_{mn}\\V_{mn}\\W_{bmn}\\W_{smn}\end{Bmatrix}=\begin{Bmatrix}0\\0\\Q_{mn}\\Q_{mn}\end{Bmatrix} \tag{17}$$

With

$$a_{11}=A_{11}\lambda^2+A_{66}\mu^2,\ a_{12}=\lambda\mu(A_{12}+A_{66}) \tag{18a}$$

$$a_{13}=-\lambda[B_{11}\lambda^2+(B_{12}+2B_{66})\mu^2],\ a_{14}=-\lambda[B_{11}^s\lambda^2+(B_{12}^s+2B_{66}^s)\mu^2] \tag{18b}$$

$$a_{22}=A_{66}\lambda^2+A_{22}\mu^2,\ a_{23}=-\mu[B_{22}\mu^2+(B_{12}+2B_{66})\lambda^2] \tag{18c}$$

$$a_{24}=-\mu[B_{22}^s\mu^2+(B_{12}^s+2B_{66}^s)\lambda^2] \tag{18d}$$

$$a_{33}=D_{11}\lambda^4+2(D_{12}+2D_{66})\lambda^2\mu^2+D_{22}\mu^4 \tag{18e}$$

$$a_{34}=D_{11}^s\lambda^4+2(D_{12}^s+2D_{66}^s)\lambda^2\mu^2+D_{22}^s\mu^4 \tag{18f}$$

$$a_{44}=H_{11}^s\lambda^4+2(H_{12}^s+2H_{66}^s)\lambda^2\mu^2+H_{22}^s\mu^4+A_{55}^s\lambda^2+A_{44}^s\mu^2 \tag{18g}$$

Table 2 FG Plate's material properties

Designation	Poisson's ratio ν	Young's modulus E (GPa)
Metal (Aluminum)	0.3	70
Ceramic (Alumina)	0.3	380

Table 3 Effect of homogeneity degree β on the displacement and stresses of a perfect square FG plate

	Micromechanical model	Theory	β=1	β =2	β=4	β=8
$\bar{W}$	Voigt	Quasi-3D (Wu *et al.* 2011)	0,5876	0,7571	0,8823	0,9739
		SSDT (Zenkour 2006)	0,5889	0,7573	0,8819	0,9750
		HSDT (Mantari *et al.* 2012)	0,5880	0,7564	0,8814	0,9737
		TSDT (Wu *et al.* 2010)	0,5890	0,7573	0,8815	0,9747
		Present	0,5889	0,7573	0,8819	0,9750
	Reuss	Present	0,8133	0,9421	1,0560	1,1783
	LRVE	Present	0,7313	0,8695	0,9749	1,0882
	Mori-Tanaka	Present	0,7628	0,8983	1,0095	1,1268
$\overline{\sigma_x}(h/3)$	Voigt	Quasi-3D (Wu *et al.* 2011)	1,5061	1,4133	1,1841	0,9622
		SSDT (Zenkour 2006)	1,4894	1,3954	1,1783	0,9466
		HSDT (Mantari *et al.* 2012)	1,4888	1,3940	1,1755	0,9431
		TSDT (Wu *et al.* 2010)	1,4898	1,3960	1,1794	0,9477
		Present	1,4894	1,3954	1,1783	0,9466
	Reuss	Present	1,2265	1,0700	0,9563	0,9156
	LRVE	Present	1,3704	1,1854	0,9906	0,8565
	Mori-Tanaka	Present	1,3009	1,1310	0,9795	0,8950
$\overline{\tau_{xz}}(h/3)$	Voigt	Quasi-3D (Wu *et al.* 2011)	0,2511	0,2495	0,2362	0,2261
		SSDT (Zenkour 2006)	0,2622	0,2763	0,2580	0,2121
		HSDT (Mantari *et al.* 2012)	0,2566	0,2741	0,2623	0,2140
		TSDT (Wu *et al.* 2010)	0,2599	0,2721	0,2519	0,2087
		Present	0,2622	0,2763	0,2580	0,2121
	Reuss	Present	0,2524	0,2378	0,2186	0,2069
	LRVE	Present	0,2665	0,2556	0,2248	0,2050
	Mori-Tanaka	Present	0,2588	0,2468	0,2237	0,2069

5. Numerical results

In this part of the manuscript, we proceed to the validation of the present theory followed by the study of the behavior of FG plates considering numerous micromechanical models; to attain this purpose, an FG plate consisting of a material combination of ceramic and metal is considered, the material properties are shown in Table 2 as follow (Daouadji *et al.* 2016b, Hadj *et al.* 2021)

$$\bar{w} = \frac{10h^3 E_c}{q_0 a^4} w\left(\frac{a}{2}, \frac{b}{2}\right), \bar{\sigma}_x = \frac{h}{q_0 a}\sigma_x\left(\frac{a}{2}, \frac{b}{2}, \frac{z}{h}\right), \bar{\tau}_{xz} = \frac{h}{q_0 a}\tau_{xz}\left(0, \frac{b}{2}, \frac{z}{h}\right), \bar{\tau}_{xy} = \frac{h}{q_0 a}\tau_{xy}\left(0,0, \frac{z}{h}\right) \quad (19)$$

Table 3 clearly illustrates the convergence between the different high order shear deformation theories Quasi-3D (Wu *et al.* 2011), SSDT (Zenkour 2006), HSDT (Mantari *et al.* 2012) and TSDT (Wu *et al.* 2010) and the present model utilizing four micromechanical models (Voigt,

Table 4 Variation of the dimensionless deflection $\overline{W}$ as a function of the side-to-thickness ratio "*a/h*" and the homogeneity degree "β" of a perfect square FG plate

a/h	Micromechanical model	Ceramic ($\beta = 0$)	β=1	β=2	β=5	β=10	Metal ($\beta = \infty$)
a/h=10	Voigt	0,2181	0,6410	0,8978	1,0659	1,0754	1,1840
	Reuss	0,2181	0,9215	1,0417	1,0893	1,1037	1,1840
	LRVE	0,2181	0,8428	1,0156	1,0781	1,0874	1,1840
	Mori-Tanaka	0,2181	0,8694	1,0214	1,0832	1,0952	1,1840
a/h=20	Voigt	0,1098	0,3218	0,4510	0,5364	0,5418	0,5961
	Reuss	0,1098	0,4632	0,5242	0,5486	0,5560	0,5961
	LRVE	0,1098	0,4234	0,5107	0,5430	0,5479	0,5961
	Mori-Tanaka	0,1098	0,4369	0,5138	0,5455	0,5518	0,5961
a/h=40	Voigt	0,0550	0,1611	0,2257	0,2687	0,2714	0,2986
	Reuss	0,0550	0,2319	0,2625	0,2748	0,2785	0,2986
	LRVE	0,0550	0,2119	0,2557	0,2720	0,2745	0,2986
	Mori-Tanaka	0,0550	0,2187	0,2573	0,2733	0,2764	0,2986
a/h=60	Voigt	0,0367	0,1074	0,1505	0,1792	0,1810	0,1991
	Reuss	0,0367	0,1547	0,1751	0,1833	0,1858	0,1991
	LRVE	0,0367	0,1413	0,1705	0,1814	0,1830	0,1991
	Mori-Tanaka	0,0367	0,1459	0,1716	0,1822	0,1843	0,1991
a/h=80	Voigt	0,0275	0,0805	0,1129	0,1344	0,1358	0,1493
	Reuss	0,0275	0,1160	0,1313	0,1375	0,1393	0,1493
	LRVE	0,0275	0,1060	0,1279	0,1361	0,1373	0,1493
	Mori-Tanaka	0,0275	0,1094	0,1287	0,1367	0,1383	0,1493
a/h=100	Voigt	0,0220	0,0644	0,0903	0,1075	0,1086	0,1195
	Reuss	0,0220	0,0928	0,1051	0,1100	0,1115	0,1195
	LRVE	0,0220	0,0848	0,1023	0,1088	0,1098	0,1195
	Mori-Tanaka	0,0220	0,0875	0,1030	0,1094	0,1106	0,1195

Reuss, LRVE, and Mori-Tanaka). As illustrated in this table, among the limitations of previous studies is the fact that they consider only one micromechanical model (Voigt) in their investigations while in the present study on the mechanical behavior of FG plates, we take in consideration four micromechanical models (Voigt, Reuss, LRVE, and Mori-Tanaka) to provide a range of potentials to engineers and researchers.

The effect of homogeneity degree β on the dimensionless deflection and stresses of a functionally graded FG plate under a transverse load is displayed in this table. It is evident that the degree of homogeneity value determines how these stresses and deflection vary, where this degree indicates the dominance of the properties of one of the components over the other, knowing that a value equal to or near zero indicates that the ceramic properties are dominant in the FG plate, on the other hand, a greater value of β is in favor of the dominance in the metal properties.

Table 4 and Figs. 2-3 exhibits the effect of micromechanical models against geometry parameters and degree of homogeneity on the dimensionless displacement (deflection) of an FG plate using the present refined shear deformation theory. It can be easily observed from the Table 4 and Figs. 2-3 that the displacement is decreasing with the increase of geometry ratios (side-to-thickness ratio *a/h* and aspect ratio *a/b*) for the different micromechanical models (Voigt, Reuss,

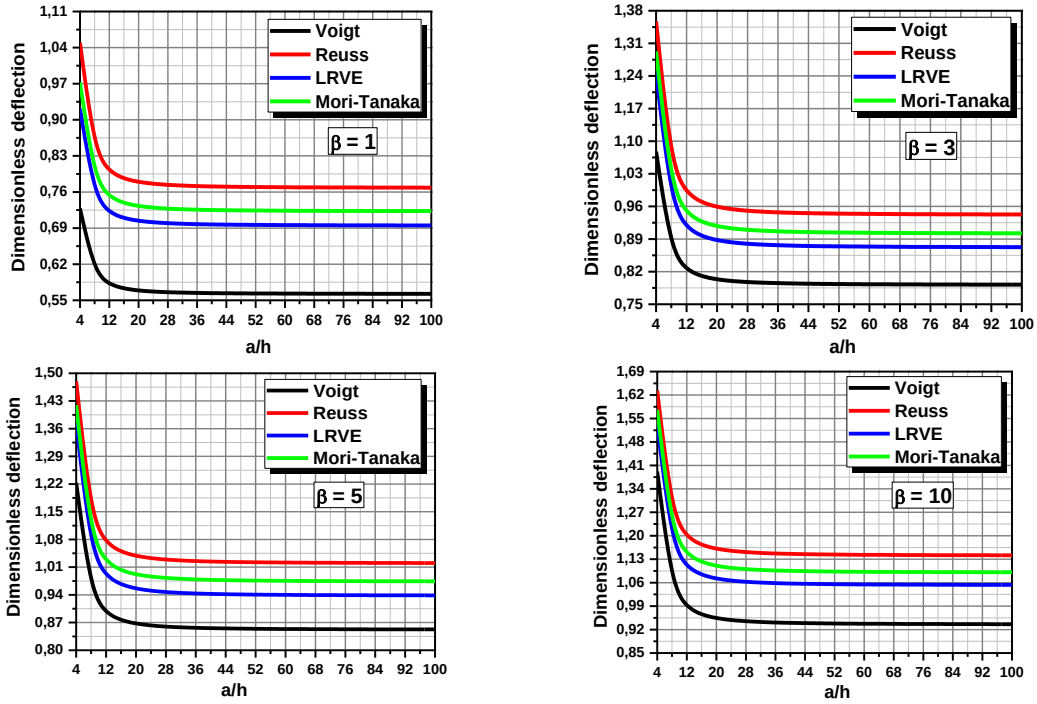

Fig. 2 Variation of the dimensionless deflection $\bar{W}$ as a function of side-to-thickness ratio "*a/h*" and the degree of homogeneity β of a perfect square FG plate

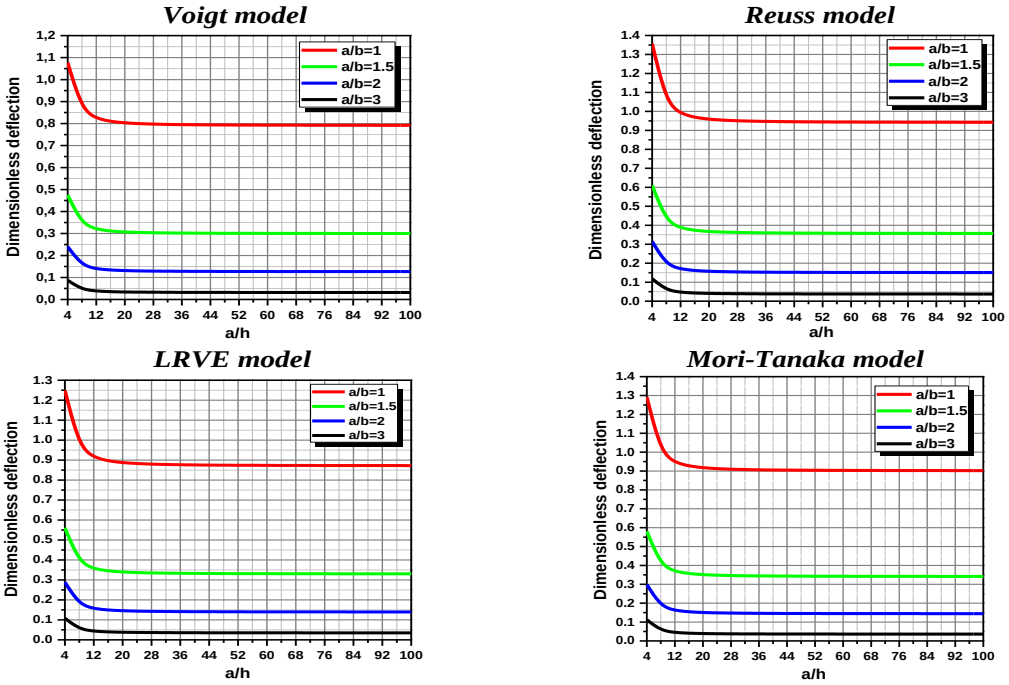

Fig. 3 Variation of the dimensionless deflection $\bar{W}$ as a function of side-to-thickness ratio "*a/h*" and the aspect ratio "*a/b*" of a perfect FG plate "β =3"

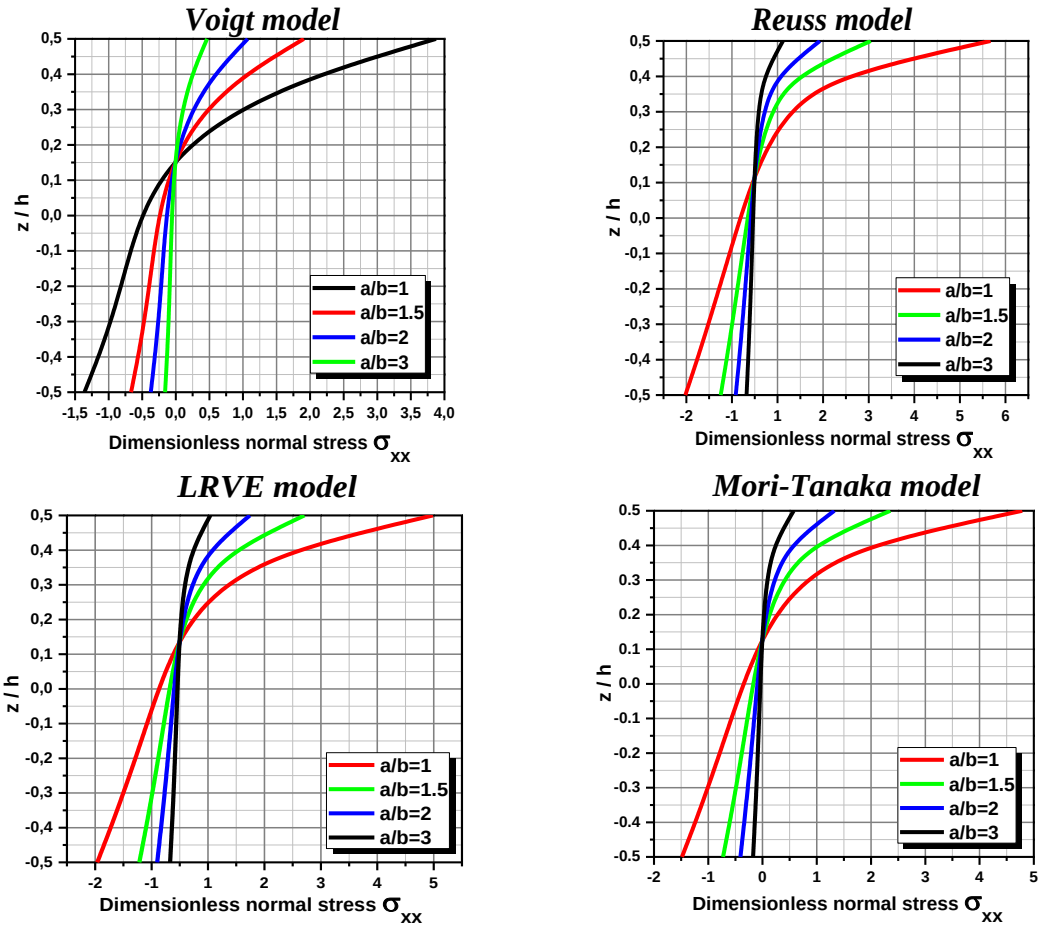

Fig. 4 Distribution of dimensionless normal stresses $\overline{\sigma_{xx}}$ through the thickness of a perfect FG plate as a function of the aspect ratio "*a/b*"

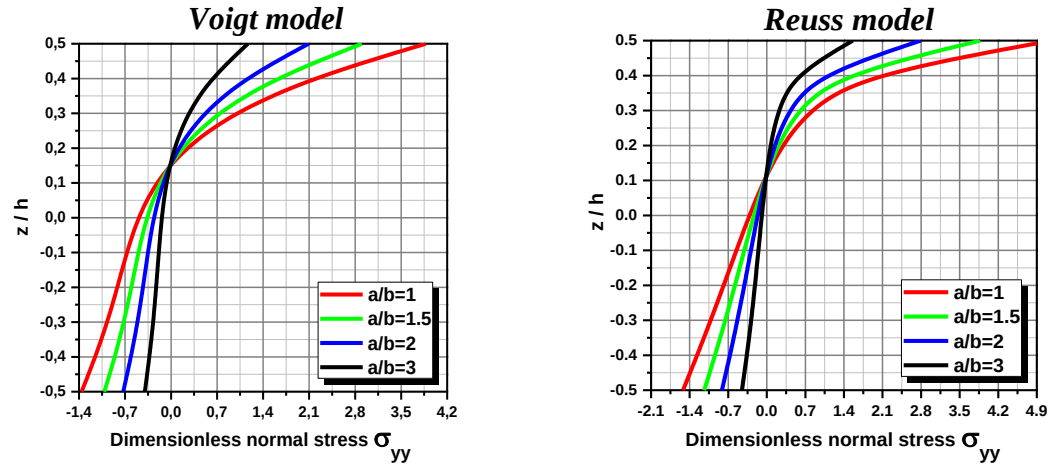

Fig. 5 Distribution of dimensionless normal stresses $\overline{\sigma_{yy}}$ through the thickness of a perfect FG plate as a function of the aspect ratio "*a/b*"

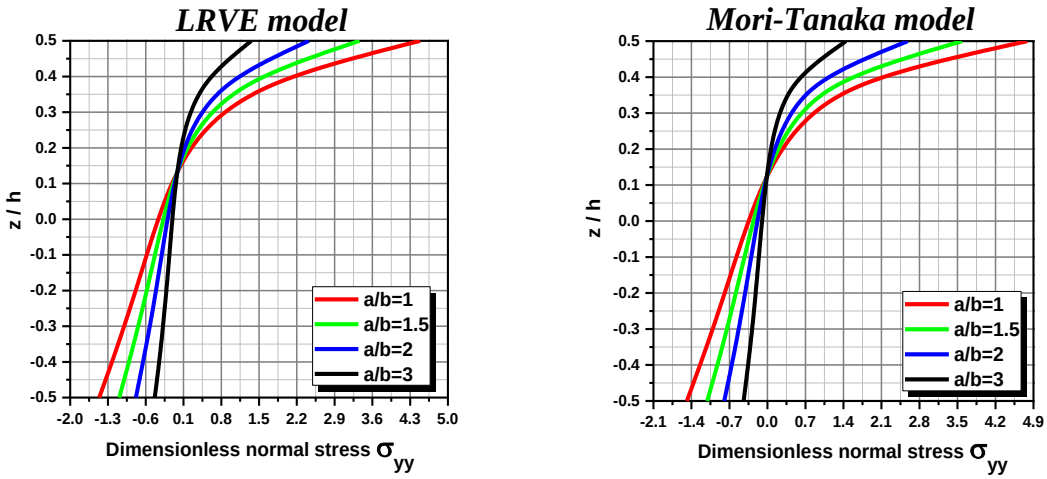

Fig. 5 Continued

LRVE ant Mori-Tanaka). Moreover, it is been observed from the results exhibited here that for all the materials combinations (different values of β), Voigt's micromechanical model underestimates the deflection while Reuss's model over estimates it, LRVE and Mori-Tanaka models gives values of deflection between those of the Voigt's and Reuss's.

Furthermore, it is evident from Figs. 2-3 that the deflection results differ from one another. This is due to the description of the variation of the Young's modulus throughout the thickness of the plate, where the micromechanical model of Voigt gives the greatest values of the Young's modulus (overestimating it) and the model of Reuss gives the smallest values (underestimating it). The results of the LRVE and Mori-Tanaka models fall between those of the two earlier models (Voigt and Reuss). In addition, in the present study we considered from the literature the simplest and widely used micromechanical models to investigate their reliability and efficiency in the study of the mechanical behavior of porous FGM plates.

Figs. 4-8 show the variation of dimensionless normal and shear stresses ($\bar{\sigma}_x$, $\bar{\sigma}_y$, $\bar{\tau}_{xy}$, $\bar{\tau}_{xz}$ and $\bar{\tau}_{yz}$) through the thickness of an FG plate as a function of the aspect ratio "*a/b*" for different micromechanical models. As presented in Figs. 4-5, the normal stresses $\bar{\sigma}_x$ and $\bar{\sigma}_y$, reaches its maximum of compression at the upper face of the plate, on the other hand it reaches its maximum of tension in the bottom face of the FG plate. Furthermore, based on Figs. 7-8, we can be irrefutably confirming the efficiency and precision of the present theory for describing the behavior of FG plates, mainly: the shear stresses distribution in a parabolic way through the FG plate's thickness and assuring the nullity of these shear stresses at the upper and lower faces of the FG plate.

Fig. 9 displays the effect of porosity distribution versus side-to-thickness on the dimensionless deflection of a square FG plate using the present theory. It can be effortlessly seen-for all micromechanical models-that the deflection is dependent on the shape of porosity distribution across the plate's thickness, where this displacement is maximal for the case of the porosity distribution in "*X*" shape (Type II), and minimal for the case of porosity distribution in form of "*V*" (Type IV), the other distribution shapes (Type I: uniform and Type III: "*O*" shape) gives results between those of the last ones while the perfect plate gives the lowest values of deflection.

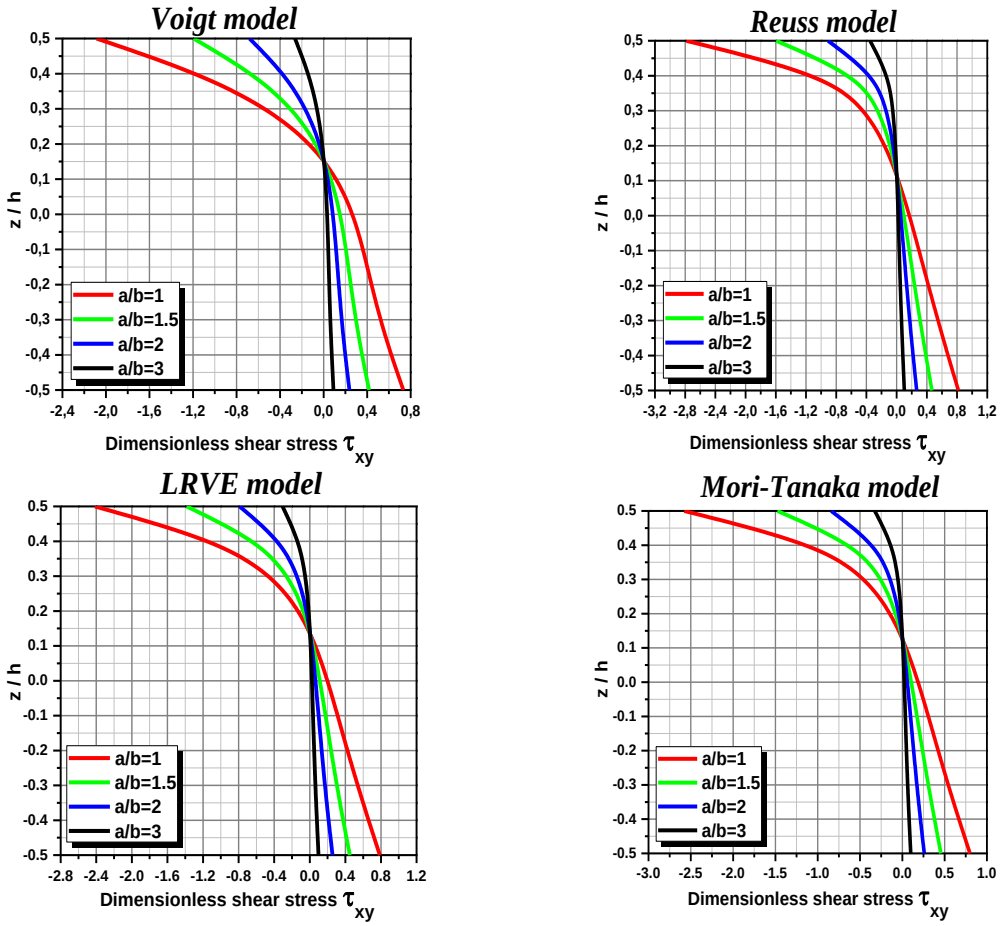

Fig. 6 Distribution of dimensionless shear stresses $\overline{\tau_{xy}}$ through the thickness of a perfect FG plate as a function of the aspect ratio "*a/b*"

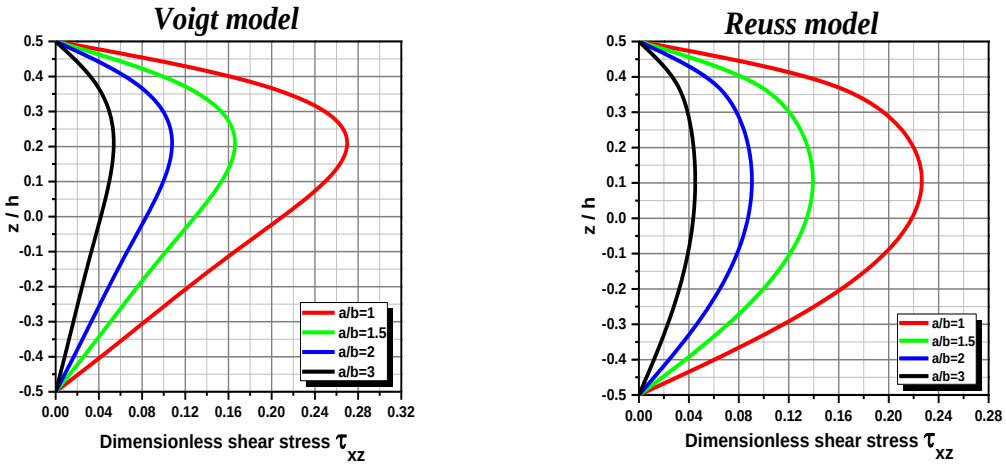

Fig. 7 Distribution of dimensionless shear stresses $\overline{\tau_{xz}}$ through the thickness of a perfect FG plate as a function of the aspect ratio "*a/b*"

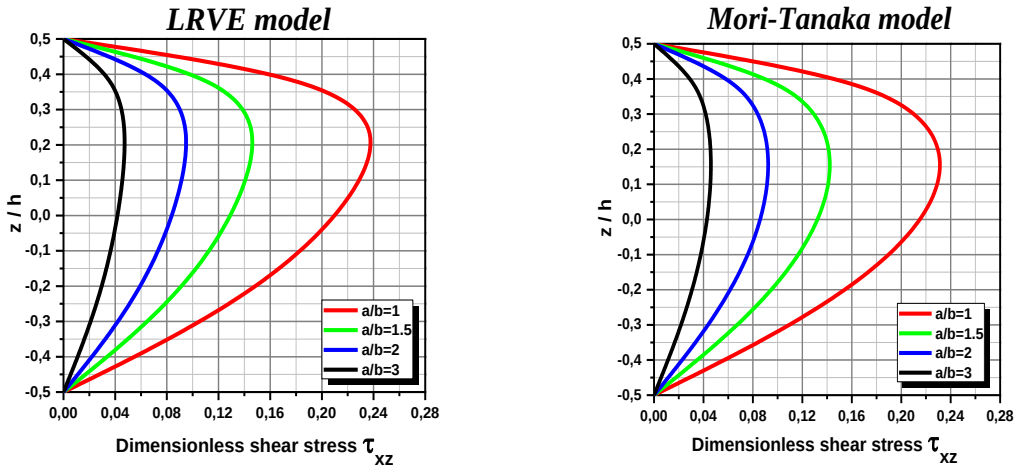

Fig. 7 Continued

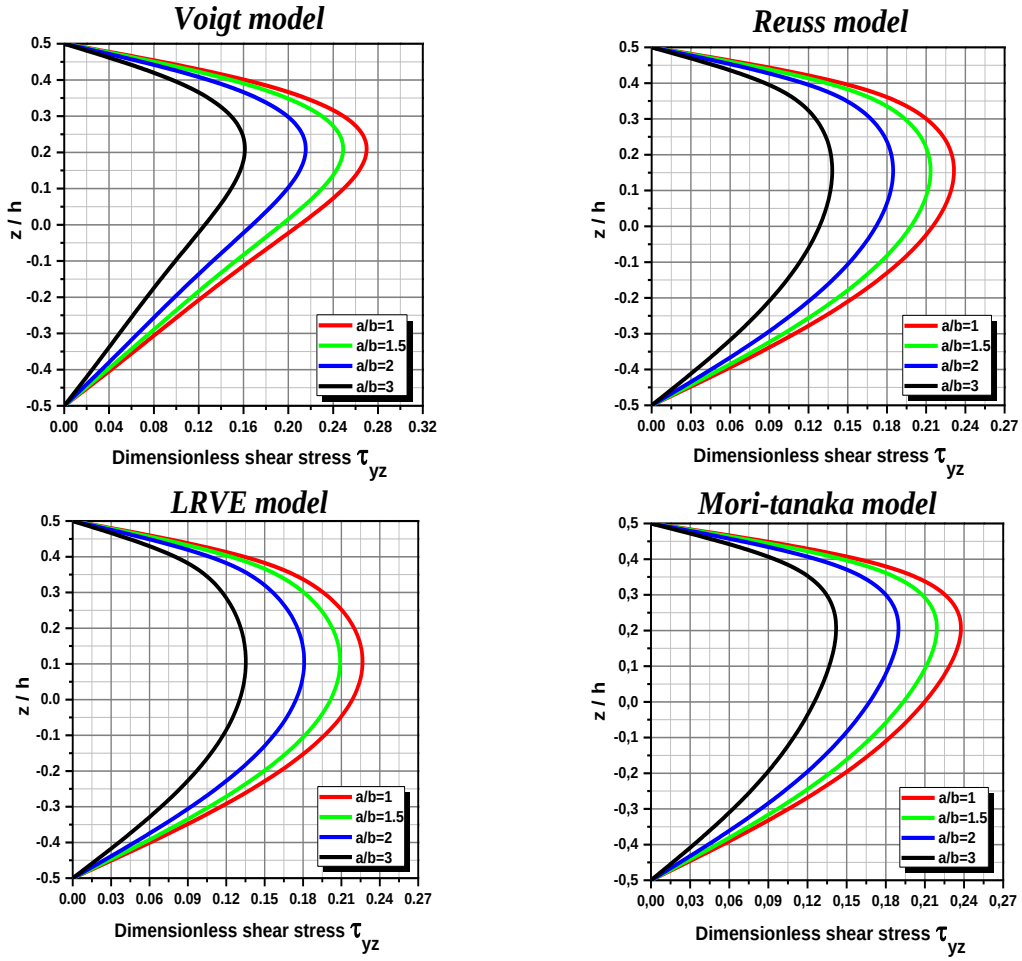

Fig. 8 Distribution of dimensionless shear stresses $\overline{\tau_{yz}}$ through the thickness of a perfect FG plate as a function of the aspect ratio "*a/b*"

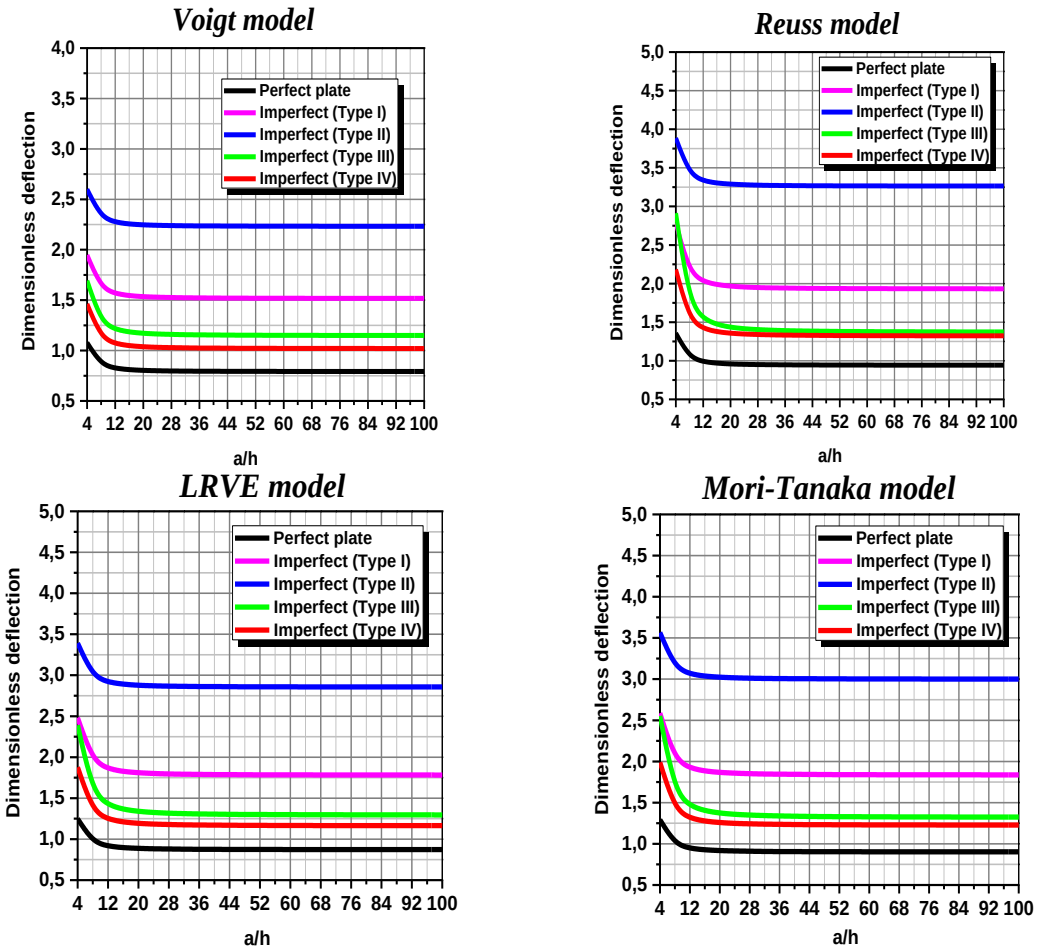

Fig. 9 Variation of the dimensionless deflection $\bar{W}$ as a function of porosity shape and side-to-thickness ratio "*a/h*" of a square FG plate "β =3"

Fig. 10 illustrate the variation of dimensionless normal stress $\bar{\sigma}_x$ through an FG plate's thickness as a function of porosity shape for various micromechanical models. As established in Fig. 10, and for all porosities distribution shapes, the normal stresses $\bar{\sigma}_x$ is maximal for the case of the Reuss micromechanical model, and minimal for the case of Voigt's model, the other micromechanical models (LRVE and Mori-Tanaka) give results between those of the last ones.

Furthermore, all forms of porosity produce almost the same stress distribution shape and values, making the impact of porosity distribution shapes on the stress distribution across the FG plate's thickness less evident.

6. Conclusions

In this study, we used an effective refined high order shear deformation theory to investigate the bending behavior of perfect/imperfect functionally graded plates. By contrasting its findings

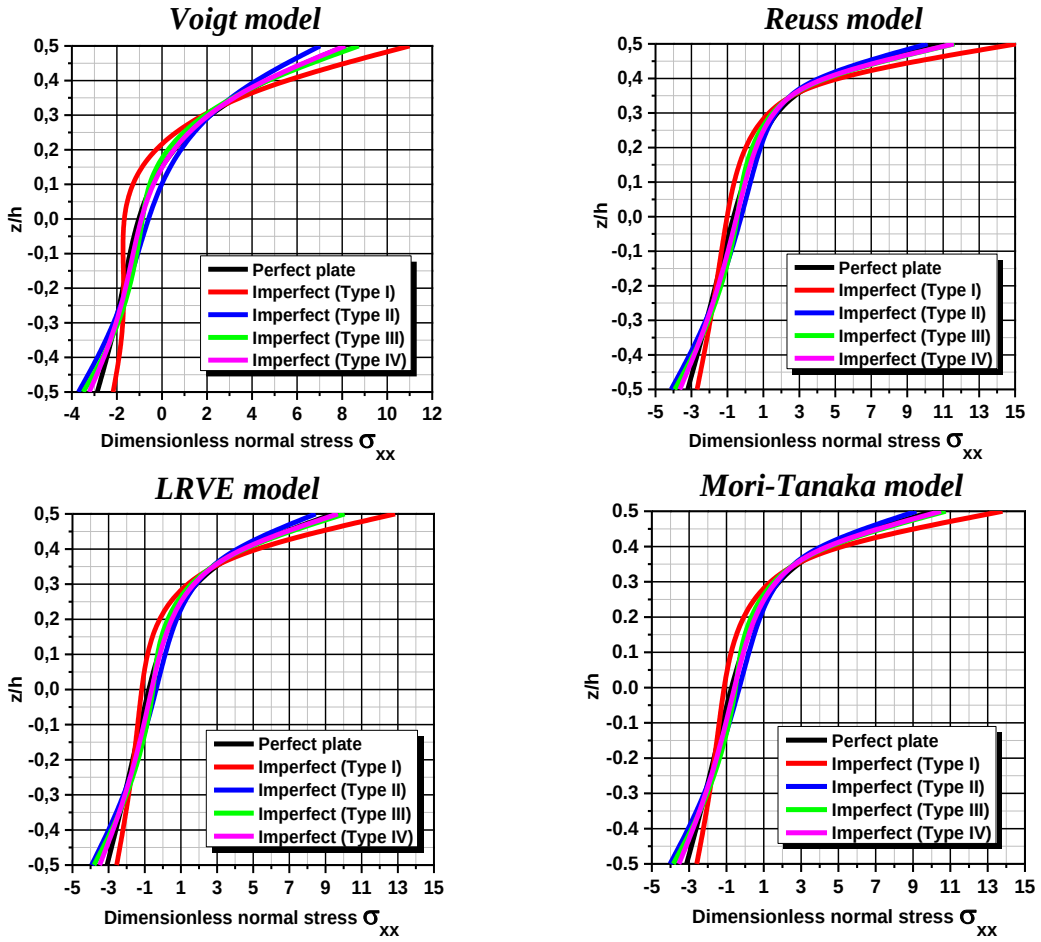

Fig. 10 Distribution of dimensionless normal stresses $\overline{\sigma_{xx}}$ through the thickness of a rectangular FG plate "*a/b*=0.5" as a function of porosity shape "β=3"

with those of other higher order theories (Quasi-3D, SSDT, HSDT and TSDT), the current theory's validity is clearly demonstrated. Following validation, a parametric study was carried out to identify the primary factors that significantly impact the FG plate's bending behavior (for stress and displacement). These factors include the material's properties (Young's modulus variation according to the homogeneity degree β), the plate's geometry (side-to-thickness ratio (*a/h*) and aspect-ratio (*a/b*)), porosity distribution shapes (Type I, Type II, Type III and Type IV) and-above all-micromechanical models' description (Voigt, Reuss, LRVE, and Mori-Tanaka).

The primary findings of this study are as follows:

- The FG plate's displacements and stresses increase as the homogeneity degree β increases;
- The deflection reduces as the aspect-ratio *a/b* and side-to-thickness ratio *a/h* increase.
- The displacement is greatly affected by micromechanical models; the LRVE and Mori-Tanaka models provide deflection values that fall between those of the Voigt and Reuss models, whereas the Voigt model underestimates the deflection and the Reuss model overestimates it.

• The porosity distribution shape has an important influence on the behavior of FG plates, which should not be taking lightly in the conception and manufacturing of this type of plates
• The current refined high order shear deformation theory provides accurate and reliable findings for all micromechanical models and porosity distribution shapes, particularly for the distribution of shear stresses over the FG plate's thickness.

The present refined high order theory can be exploited in future researches in the field of functionally graded plates (for perfect or porous plates), for instance, we can investigate using other micromechanical models and their implications in diverse loading conditions (mechanical, thermal and hygro-thermo-mechanical loadings), or in studying the buckling and vibration behavior of porous FG plates using micromechanical models and for various porosity distribution shapes.

References

Abouelregal, A.E. (2022), "Generalized thermoelastic MGT model for a functionally graded heterogeneous unbounded medium containing a spherical hole", *Eur. Phys. J. Plus*, **137**(8), 953. https://doi.org/10.1140/epjp/s13360-022-03160-1.

Abouelregal, A.E. and Dargail, H.E. (2023), "Memory and dynamic response of a thermoelastic functionally graded nanobeams due to a periodic heat flux", *Mech. Bas. Des. Struct. Mach.*, **51**(4), 2154-2176. https://doi.org/10.1080/15397734.2021.1890616.

Abouelregal, A.E. and Mohamed, B.O. (2018), "Fractional order thermoelasticity for a functionally graded thermoelastic nanobeam induced by a sinusoidal pulse heating", *J. Comput. Theor. Nanosci.*, **15**(4), 1233-1242. https://doi.org/10.1166/jctn.2018.7209.

Adim, B. and Daouadji, T.H. (2024), "Analysis of buckling behavior of functionally graded plates under mechanical loading", *J. Nano-Electr. Phys.*, **16**(2), 02003. https://doi.org/10.21272/jnep.16(2).02003.

Adim, B., Daouadji, T.H. and Rabahi, A. (2016), "A simple higher order shear deformation theory for mechanical behavior of laminated composite plates", *Int. J. Adv. Struct. Eng. (IJASE)*, **8**(2), 103-117. https://doi.org/10.1007/s40091-016-0109-x.

Adiyaman, G. and Turan, M. (2024), "Bending and buckling analysis of porous 2D functionally graded beams with exponential material property variation", *Iran. J. Sci. Technol., Tran. Civil Eng.*, 1-28. https://doi.org/10.1007/s40996-024-01508-4.

Alsaeed, S.S. and Abouelregal, A.E. (2025), "Analysis of thermomechanical responses of functionally graded unbounded materials using an advanced dual-phase delay heat transfer model with higher-order fractional derivatives", *ZAMM-J. Appl. Math. Mech./Zeitschrift für Angewandte Mathematik und Mechanik*, **105**(1), e202400930. https://doi.org/10.1002/zamm.202400930.

Amir, M., Kim, S.W. and Choi, D. (2024), "Comparative static analysis of functionally graded porous curved beams: Deterministic versus stochastic approaches", *Jo. Strain Anal. Eng. Des.*, **59**(8), 559-574. https://doi.org/10.1177/03093247241273794.

Billel, R. (2023), "Contribution to study the effect of (Reuss, LRVE, Tamura) models on the axial and shear stress of sandwich FGM plate (Ti-6A1-4V/ZrO 2) subjected on linear and nonlinear thermal loads", *AIMS Mater. Sci.*, **10**(1), 26-39. https://doi.org/10.3934/matersci.2023002.

Bouazza, M., Amara, K.H. and Zidour, M. (2024), "Employing an analytical method for post-buckling analysis of functionally graded beams", *Adv. Aircraft Spacecraft Sci.*, **11**(4), 299-312. https://doi.org/10.12989/aas.2025.11.4.299.

Bui, T.T.H., Tran, T.T.H. and Nguyen, D.K. (2021), "Geometrically nonlinear behaviour of functionally graded beam and frame structures under mechanical loading", *Regional Conference in Mechanical Manufacturing Engineering*, 326-342, Singapore. https://doi.org/10.1007/978-981-19-1968-8_26.

Chen, H.Y., Li, W. and Zhang, J.N. (2024), "Effect of micromechanical models on mechanical behavior of

functionally graded plates based on a quasi-3D hyperbolic shear deformation theory", *Int. J. Acoust. Vib.*, **29**(2), 161. https://doi.org/10.20855/ijav.2024.29.22045.

Chen, S., Geng, R. and Li, W. (2021), "Vibration analysis of functionally graded beams using a higher-order shear deformable beam model with rational shear stress distribution", *Compos. Struct.*, **277**, 114586. https://doi.org/10.1016/j.compstruct.2021.114586.

Daouadji, T.H. and Adim, B. (2016), "An analytical approach for buckling of functionally graded plates", *Adv. Mater. Res.*, **5**(3), 141-169. https://doi.org/10.12989/amr.2016.5.3.141

Daouadji, T.H., Benferhat, R. and Adim, B. (2016a), "Bending analysis of an imperfect advanced composite plates resting on the elastic foundations", *Couple. Syst. Mech.*, **5**(3), 269-283. https://doi.org/10.12989/csm.2017.5.3.269.

Daouadji, T.H., Chedad, A. and Adim, B. (2016b), "Interfacial stresses in RC beam bonded with a functionally graded material plate", *Struct. Eng. Mech.*, **60**(4), 693-705. https://doi.org/10.12989/sem.2016.60.4.693.

Gawdzińska, K., Jackowski, J. and Szweycer, M. (2001), "Odmiany porowatości odlewów z metalowych kompozytów nasycanych", *Kompozyty*, **1**(1), 68-71.

Ghazzawi, S.M. and Abdelrahman, W.G. (2020), "Static analysis of thick functionally graded plates with different property distribution functions", *Arab. J. Sci. Eng.*, **45**(7), 5099-5108. https://doi.org/10.1007/s13369-020-04344-6.

Hadj, B., Rabia, B. and Daouadji, T.H. (2021), "Vibration analysis of porous FGM plate resting on elastic foundations: Effect of the distribution shape of porosity", *Couple. Syst. Mech.*, **10**(1), 61-77. https://doi.org/10.12989/csm.2021.10.1.061.

Henni, M.A.B., Abbès, B., Daouadji, T.H., Abbès, F. and Adim, B. (2021), "Numerical modeling of hygrothermal effect on the dynamic behavior of hybrid composite plates", *Steel Compos. Struct.*, **39**(6), 751-763. https://doi.org/10.12989/scs.2021.39.6.751.

Joshi, K.K., Kar, V.R., Ghatage, P.S. and Layek, R.K. (2022), "Multi-directional graded composites: An introduction", *Advanced Composite Materials and Structures*, CRC Press.

Kim, J. and Reddy, J.N. (2013), "Analytical solutions for bending, vibration, and buckling of FGM plates using a couple stress-based third-order theory", *Compos. Struct.*, **103**, 86-98. https://doi.org/10.1016/j.compstruct.2013.03.007.

Li, W., Chen, H., Chen, S. and Liu, Z. (2025), "A force-based beam element model based on the modified higher-order shear deformation theory for accurate analysis of FG beams", *Struct.*, **71**, 107991. https://doi.org/10.1016/j.istruc.2024.107991.

Li, W., Gao, W. and Chen, S. (2020), "A material-based higher-order shear beam model for accurate analyses of FG beams with arbitrary material distribution", *Compos. Struct.*, **245**, 112253. https://doi.org/10.1016/j.compstruct.2020.112253.

Li, W., Liu, Z. and Chen, S. (2024), "A modified quasi-3D theory and mixed beam element method for static behaviour analysis of functionally graded beams", *Thin Wall. Struct.*, **204**, 112316. https://doi.org/10.1016/j.tws.2024.112316.

Li, W., Ma, H. and Gao, W. (2019), "A higher-order shear deformable mixed beam element model for accurate analysis of functionally graded sandwich beams", *Compos. Struct.*, **221**, 110830. https://doi.org/10.1016/j.compstruct.2019.04.002.

Mantari, J.L., Oktem, A.S. and Soares, C.G. (2012), "Bending response of functionally graded plates by using a new higher order shear deformation theory", *Compos. Struct.*, **94**(2), 714-723. https://doi.org/10.1016/j.compstruct.2011.09.007.

Masmoudi, F., Tamrabet, A., Refrafi, S., Alselami, N., Menasria, A., Bouhadra, A. and Benyoucef, S. (2024), "Coupled loading hygro-thermo-mechanical Effect on the stability of imperfect functionally graded sandwich plates", *J. Comput. Appl. Mech.*, **55**(4), 617-635. https://doi.org/10.22059/jcamech.2024.374122.1007.

Nadiia, D. and Jia, Q. (2024), "Effect of porous defects on mechanical behavior of functionally graded materials", *J. Strain Anal. Eng. Des.*, **60**(2), 106-116. https://doi.org/10.1177/03093247241287951.

Naebe, M. and Shirvanimoghaddam, K. (2016), "Functionally graded materials: A review of fabrication and

properties", *Appl. Mater. Today*, **5**, 223-245. https://doi.org/10.1016/j.apmt.2016.10.001

Naveen K.S.N. and Devarajaiah R.M. (2024), *Functionally Graded Materials*, Futuristic Trends in Mechanical Engineering Book 5, Volume 3, IIP Series.

Njim, E.K., Sadiq, S.E., Tahir, M.A.D., Flayyih, M.A. and Hadji, L. (2023), "Flexural bending and fatigue analysis of functionally graded viscoelastic materials: experimental and numerical approaches", *Phys. Chem. Solid State*, **24**(4), 628-639. https://doi.org/10.15330/pcss.24.4.628-639.

Noori, M., Bilgin, A., Diallo, H., Al Rousan, M.O. and Noorı, A.R. (2024), "A study on the influence of material gradient index on bending and stress responses of FGM rectangular plates using the Finite Element Method", *J. Sustain. Constr. Mater. Technol.*, **9**(3), 239-254. https://doi.org/10.47481/jscmt.1555157.

Sahmani, S., Safaei, B. and Aldakheel, F. (2021), "Surface elastic-based nonlinear bending analysis of functionally graded nanoplates with variable thickness", *Eur. Phys. J. Plus*, **136**, 1-28. https://doi.org/10.1140/epjp/s13360-021-01667-7.

Sidda R.B. and Vijaya K.R.K. (2024), "Analyzing the buckling behavior of in-plane bidirectional functionally graded porous plates", *J. Comput. Appl. Mech.*, **55**(3), 322-339. https://doi.org/10.22059/jcamech.2024.373641.995.

Silva, R.F., Coelho, P.G., Gustavo, C.V., Almeida, C.J., Farias, F.W.C., Duarte, V.R., ... & Santos, T.G. (2024), "Functionally graded materials and structures: Unified approach by optimal design, metal additive manufacturing, and image-based characterization", *Mater.*, **17**(18), 4545. https://doi.org/10.3390/ma17184545.

Son, T. and Qui, L.X. (2022), "Investigate the bending and free vibration responses of multi-directional functionally graded plates with variable thickness based on isogeometric analysis", *J. Sci. Technol. Civil Eng. (JSTCE)-HUCE*, **16**(4), 10-29. https://doi.org/10.31814/stce.nuce2022-16(4)-02.

Wu, C., Zhang, L., Weng, G.J. and Yin, H. (2024), "Thermomechanical modeling of functionally graded materials based on bimaterial fundamental solutions", *Int. J. Eng. Sci.*, **198**, 104040. https://doi.org/10.1016/j.ijengsci.2024.104040.

Wu, C.P. and Li, H.Y. (2010), "An RMVT-based third-order shear deformation theory of multilayered functionally graded material plates", *Compos. Struct.*, **92**(10), 2591-2605. https://doi.org/10.1016/j.compstruct.2010.01.022.

Wu, C.P., Chiu, K.H. and Wang, Y.M. (2011), "RMVT-based meshless collocation and element-free Galerkin methods for the quasi-3D analysis of multilayered composite and FGM plates", *Compos. Struct.*, **93**(2), 923-943. https://doi.org/10.1016/j.compstruct.2010.07.001.

Zaoui, F.Z., Ouinas, D., Achour, B., Touahmia, M., Boukendakdji, M., Latifee, E.R., ... & Viña Olay, J.A. (2022), "Mathematical approach for mechanical behaviour analysis of FGM plates on elastic foundation", *Math.*, **10**(24), 4764. https://doi.org/10.3390/math10244764.

Zenkour, A.M. (2006), "Generalized shear deformation theory for bending analysis of functionally graded plates", *Appl. Math. Model.*, **30**(1), 67-84. https://doi.org/10.1016/j.apm.2005.03.009.

Zghal, S. and Dammak, F. (2024), *Functionally Graded Materials: Analysis and Applications to FGM, FG-CNTRC and FG Porous Structures*, CRC Press.

CC